Mechanical relaxation spectroscopy of chalcogenide glasses

V. I. MIKLA*, A. A. HORVAT, A. E. KRISHTOFORY, V. V. MINKOVICH
Institute for Solid State Physics and Chemistry, Uzhgorod National University, Uzhgorod, Voloshina St. 54, Ukraine

Basic fundamentals of the elastic behavior of a standard linear solid and the internal friction technique based on this model are briefly described. The internal friction (Q^{-1}) caused by various thermally activated processes in vitreous solids are reviewed for several glass compositions in relation to atomic mobility and other relevant properties. A similar relaxation mechanism is the inherent feature of different vitreous solids. The present authors suggest that the mechanisms responsible for the internal friction peaks in selenium-based glasses are closely related to the polymeric structure. These peaks exist in many polymers and may be considered as they universal feature.

(Received January 10, 2011; accepted January 26, 2011)

Keywords: Mechanical stress, Internal friction, Structural relaxation, Chalcogenide glasses

1. Introduction

In the last 10 years there has been a renewed interest in amorphous chalcogenides due to their applications as an X-ray photoconductors in a new generation of digital detectors for medical X-ray imaging and diagnostics [1-3]. This leads to further development of a relatively new branch in medical science which is known today as Diagnostic Radiology (DR). DR always was and still is a dynamically developing part of medical practice. Such a rapid development is due mainly to two reasons: the constant need of high quality images containing as much diagnostic information as possible and the need to obtain the diagnostic information with as little x-ray exposure of the patient as possible. Due to their higher resolution, lower X-ray dose amorphous chalcogenides are very promising and have no competitors among other solid state materials.

Although amorphous selenium (a-Se) is one of the earliest and most widely used amorphous semiconductor, and in spite of its use as the standard model system in the general discussion of molecular structure of chalcogenide glasses, many of the properties of a-Se have not been fully explored or understood to date.

The study of As_xSe_{1-x} glasses is interesting since the atoms of As crosslink the polymeric chains of a-Se. Recently, the effect of As alloying was re-examined in numerous publications. Corresponding data were systematized in [4,5]. Although the general trends on the effect of As alloying are generally known and dates back to the 1970s, the selenium alloying technology is far from the exact science of the crystalline silicon technology in terms of scientific understanding and reproducibility. There is a strong dependence of structure and various physical properties of a given Se alloy on the preparation technology. This may be due to the great variability of the structure of selenium.

With the renewed interest in a-Se that has been generated recently, as mentioned above by the use of a-Se for X-ray imaging applications, we have decided to examine some of the unresolved issues. Specifically, the aim of present review of experimental data on tensile mechanical stress and internal friction techniques is to clarify mechanical response of glasses following external perturbation. Clearly, the classical methods for structural studies are usually diffraction experiments. These techniques are not always sufficiently sensitive to discuss the short-range order or even structural defects in amorphous materials. Less familiar indirect methods which deal with the measurements of structure-sensitive properties, such as mechanical stress, internal friction, are therefore of great importance.

The internal friction and the dynamic modulus are the most basic of all mechanical properties, and their importance in any application is well-known. Either internal friction or modulus of a given material is sensitive, not only to many kinds of molecular motion, but also to various transitions, relaxation processes, structural heterogeneities and the morphology of multiphase system. Therefore, interpretations of the dynamic mechanical properties at the molecular level are of great scientific and practical importance in understanding the mechanical behavior of solids with polymer-like structure.

2. Theoretical framework

If a solid in thermodynamic equilibrium is suddenly subjected to a change in external conditions, it must achieve a new state of equilibrium consistent with the new conditions. This readjustment process, in other words relaxation, commonly occurs in nature. In the following discussion we restrict ourselves on recoverable anelastic effects that originate from rearrangement of the atomic

configuration under the influence of an applied stress, although diffusional, thermal, dielectric and magnetic relaxation are analogous phenomena.

Recoverable anelasticity implies that, when a stress is applied to a solid, the free energy increases due to slight displacements of atoms from their equilibrium positions. For an energy barrier to be overcome, a certain time is required fro the completion of the process. As a result, the maximum strain is delayed with respect to the maximum applied stress. When the stress is removed, the deformation is fully recovered by thermal motion.

A mechanical model [6], termed standard linear solid, consisting of two perfectly elastic springs (stiffness constants C_1 and C_2) and a dashpot (inertia member with a viscous flow constant 1/η) satisfactorily describes the anelastic behavior of many solids. The linear differential equation describing this model is:

$$F\left(\frac{1}{C_1}+\frac{1}{C_2}\right)+\frac{\tau}{C_1}\frac{dF}{dt}=x+\tau\frac{dx}{dt} \qquad (1)$$

where F is the applied force (stress) and x is the total displacement (strain). When a relaxation time τ is defined as $\eta \equiv \tau C_2$, and C_1 and C_2 are replaced by un-relaxed and relaxed compliances $S_u = 1/C_1$ and $S_x = 1/C_1 + 1/C_2$, respectively, Eq. 1 becomes:

$$S_x F + \tau S_u \frac{dF}{dt} = x + \tau \frac{dx}{dt} \ . \qquad (2)$$

For the stress (F) and strain (x) varying periodically, one can obtained the following expression for the loss tangent from Eq. 2:

$$\tan\delta = \frac{(S_x - S_u)\omega\tau}{S_x + S_u\omega^2\tau^2} \qquad (3)$$

where ω is the angular frequency. The relaxation strength (the relaxation ratio) $\Delta = (S_x - S_u)/S_u$ is often <<1 in many solids. Reasonably, Eq. 3 commonly reduces to:

$$\tan\delta \cong \delta = \Delta\frac{\omega\tau}{1+\omega^2\tau^2} \ . \qquad (4)$$

Tan δ is a symmetrical function of ωτ with $\delta_{max} = \Delta/2$ centered at ωτ =1. Tan δ asymptotically approaches 0 as ωτ → 0, since atomic motion keeps strain and stress in phase (relaxed, isothermal conditions).

As ωτ → ∞, atom motion is unable to relax the anelastic strain and, thus, δ→ 0.

The width of the tan δ peak at half maximum is ideally $(\log\omega\tau)_2 - (\log\omega\tau)_1 = 1.414$, but the actual peak width observed in many solids is often much larger (2 to 3 times for glasses). For relaxation strengths more than 10% a change in peak shape will occur and one can account for the modulus variation due to the relaxation.

For a thermally activated process the relaxation time, τ, varies as:

$$\tau = \tau_0 \exp(U/RT) \qquad (5)$$

where R and T have their usual meaning and U is an activation energy. By measuring the peak temperature (i.e., where $\omega\tau = 1$) for several frequencies, U can be calculated from

$$U = R\frac{\ln\omega_1 - \ln\omega_2}{1/T_2 - 1/T_1} \ . \qquad (6)$$

Tan δ, commonly called internal friction, is also referred as Q^{-1} because of its electrical analogue. Physically, it is a measure of the absorption of vibrational energy in a solid and is related, therefore to the acoustic, optical, dielectric and magnetic spectrum. Experimentally Q^{-1} can be determined from the logarithmic decrement λ of a freely vibrating solid:

$$Q^{-1} = \tan\delta = \frac{2.303\lambda}{\eta\pi} \qquad (7)$$

Where $\lambda = ln\ A_0/A_n$; A_0 is the initial amplitude and A_n is the amplitude after n cycles.

Some solids are described well by the standard linear model. At the same time, most solids and, especially glasses, are better represented by models which are based on assumption of existence of spectra of τ. In such a case Eq. 3 must be summed over the various values of τ in order to account for the experimentally observed broadening in tan δ peaks. This distribution in τ results from a distribution in the activation energy (barrier heights) and related to the disorder in vitreous solids.

Generally, in vitreous solids the primary atomic processes producing characteristic tan δ peaks are:

(a) the stress-induced motion of cations
(b) interactions between different cations and between cations and protons
(c) the motion of single-bonded oxygen ions
(d) the viscoelastic character of the network.

Tan δ increases in going from crystalline solids, to glasses and to polymers. The internal friction value is: 10^{-6} for quartz, 10^{-5} to 10^{-3} for metals, 10^{-2} for most glasses and 10^{-2} to 10 for high polymers [7].

3. Techniques for measuring relaxation spectra

The choice of suitable method depends on:

(a) the magnitude of internal friction
(b) the shape and size of the specimens available
(c) the desired mode of vibration.

In broad terms, measurements can be performed in the range:

(a) 0.1 to 250 Hz – torsion oscillations of a fiber
(b) 1 to 50 kHz – flexural vibrations of a bar
(c) 10 to 110 kHz – longitudinal vibrations
(d) > attenuation of ultrasonic stress waves.

For glasses, measurement of the gradual decay in amplitude of free torsion vibrations at ~ 1 Hz is the most commonly used technique. A glass fiber suspended vertically with its lower end freely oscillating (torsion) constitutes the pendulum's anelastic member. The fiber can be surrounded by heating or cooling coils and the entire assembly placed in a vacuum chamber to eliminate air damping. The decay of the torsion oscillations is recorded in several ways (e.g., by measuring the time a beam of light, reflected from a mirror, attached to the bottom of the pendulum, passes between 2 photocells connected to an electronic timer). The reader may find various pendulum designs as well as the theoretical and experimental aspects of the procedures in the extensive literature on the topic [8-12].

For measurements of internal friction and shear module at low and infra-low frequencies (0.01-1 Hz) the method of inverted torsion pendulum is the most commonly used technique. The technique allows to studying the above physical parameters in temperature range of 77-600 K for values of mechanical strain $\sigma < 10^7$ Pa and amplitudes of relative deformation $\varepsilon \approx 10^{-6}$-$10^{-1}$. The relationship between ***external mechanical perturbation*** and the ***resulting time-dependent response*** is illustrated in Figure 1 (after Magalas [12]). Clearly, the following relationships can be analyzed: (1) between the real (in-phase) and imaginary part (out-of-phase) of compliance via the Hilbert transform **H** (Kramers-Kronig relation), (2) between the real and imaginary parts of complex compliance and the response function via the Fourier cosine $\mathbf{F_C}$ and sine $\mathbf{F_s}$ transforms, and (3) between the relaxation function and complex compliance via the Fourier transform **F** .

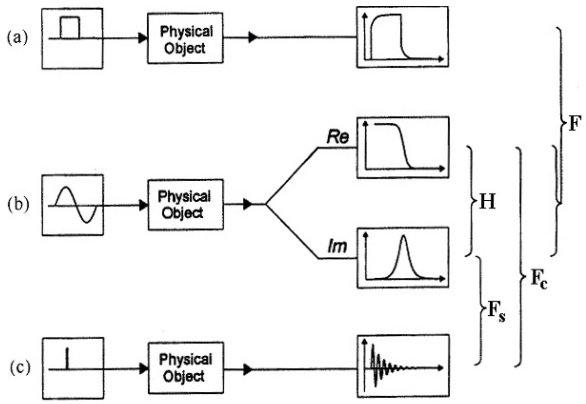

Fig. 1. Principle of mechanical relaxation measurement in the low frequency range for the case of quasi-static (a), harmonic (b) and pulsed (c) perturbation

To minimize deviations and errors it is necessary to perform Fourier transformation

$$\varepsilon(\omega) = \sum_{n=1}^{N} \varepsilon(n\Delta)\exp(-j\omega n\Delta) \tag{8}$$

with the time interval Δ and appropriate number of terms *N*. Examples of Δ for different time range are given below

$$\Delta = \begin{array}{ll} 1\text{ s}, & 1\text{ s} < t < 10^2\text{ s}, \\ 2\text{ s}, & 10^2\text{ s} < t < 10^3\text{ s}, \\ 20\text{ s}, & 10^3\text{ s} < t < 10^4\text{ s}, \\ 200\text{ s}, & 10^4\text{ s} < t. \end{array}$$

Equation for the transformation is

$$\varepsilon(\omega) = \sum_{n=0}^{100}\{\varepsilon(n)\exp(-j\omega n) + \varepsilon(n+1)\exp[-j\omega(n+1)]\}/2 + \sum_{n=0}^{449}\{\varepsilon(100+2n)\exp[-j\omega(100+2n)] + \varepsilon(100+2n+2)\exp[-j\omega(100+2n+2)]\}/2 +$$
$$+ 20\sum_{n=1}^{449}\{\varepsilon(100+20n)\exp[-j\omega(1000+20n)] + \varepsilon(1000+20n+20)\exp[-j\omega(1000+20n+20)]\}/2 +$$
$$+ 200\sum_{n=1}^{k}\{\varepsilon(10000+200n)\exp[-j\omega(10000+200n)] + \varepsilon(10000+200n+200)\exp[-j\omega(10000+200n+200)]\}/2$$

The measuring system for investigation of mechanical relaxation in glasses at infra-low frequencies is based on inverted torsion pendulum method and shown in Fig. 2.

Details of the magnetostrictive system were described in [13, 14]. In this system a generated burst of mechanical oscillations is used to excite the tested glass specimen, along its main length at either the natural frequency or one of the harmonic frequencies of the specimen. The resultant signal echo recorded by the system is shown in Figure 3. The establishment of this echo has been described in general in [15]. It is a combination of two parts: **(1)** the echo signal from the resonator specimen and the background signal from the interface between the specimen and the transmission wire-line. These two signals are in reverse phase to each other; consequently, they form a cross-over at a stage when they have the same amplitude.

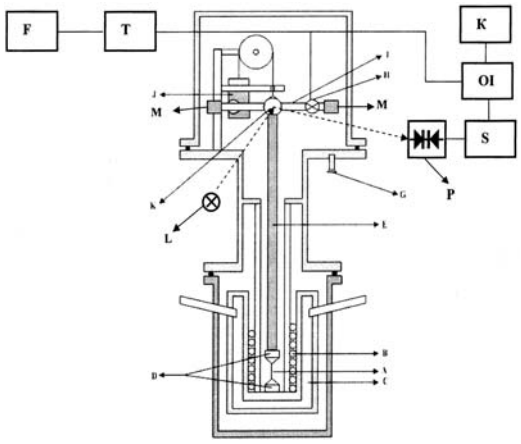

Fig. 2. Schematic illustration of inverted pendulum technique [12]

This cross-over confirms the adhesion of the specimen and the coupled line by the cementing agent and it indicates that the frequency of the transmitted signal is equal to either the natural frequency, or one of the higher mode frequencies of the specimen; and **(2)** the echo decrement which is the exponential radiation of the stored energy due to the resonator and follows the echo-signal [15].

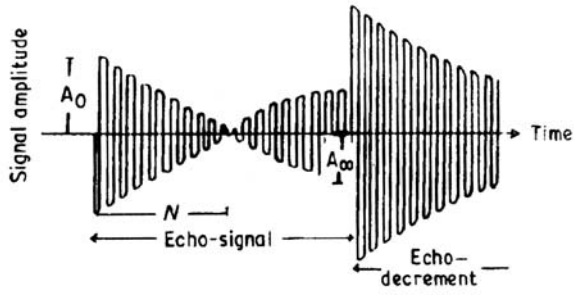

Fig. 3. Diagram of the echo-patterns displayed in the magnetostrictive delay-time system [15].

The parameters shown in Figure 3 are used to calculate the internal friction, Q^{-1}, according to the following equations [15]

$$\frac{Q_c}{Q_m} = \frac{A_0 + A_\infty}{A_0 - A_\infty} = y \tag{9}$$

$$\frac{\pi N}{Q_c} = \frac{\ln[2/(1-y]}{1+y} \tag{10}$$

where Q_c and Q_m are the coupling and the material Q-factors, respectively, A_0 and A_∞ are the initial and steady-state amplitudes of the echo-signal and N is the number of oscillations to cross-over. After recording the readings of A_0 , A_∞ and N, one can calculate the corresponding internal friction values.

A conventional ultrasonic pulse method (measurements of the attenuation of ultrasonic stress waves) [16] is used in high-frequency (100 MHz range) experiments. Particular attention should be paid to accuracy while measuring the attenuation of longitudinal waves in the specimen. This can be easily achieved if the input signal is constantly monitored and kept at a constant level.

A resonant method is used at 10 kHz frequency range [17]. Experimental set-up is displayed in Fig. 4.

Vitreous sample is shaped into a well-defined parallelepiped. Non-resonant piezoelectric quartz generate in the sample longitudinal vibrations. The natural low-frequency modes of the sample and the fundamental resonant frequency of the quartz do not interfere because the latter is 10 MHz. Supports are located on the nodes of the fundamental longitudinal vibrations. The vibrations are detected with an electrostatic method.

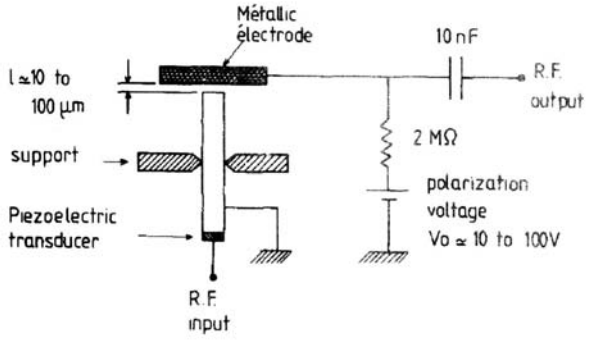

Fig. 4. Arrangement for the piezoelectric drive and electrostatic detection of forced longitudinal vibration at 10 kHz frequency [18].

The detection capacitor is formed by the sample and a metallic plane of 10-100 μm thickness parallel to it. The polarization circuitry is also shown (Fig. 4). The time constant of the circuit is much longer than the period of vibration of the sample. The RF output (δv) is related to the vibration (δx) of the sample: $\delta v = (V_0/I)\times\delta x$. The RF output is fed into a high impedance input amplifier and the signal is then recorded with a waveform digitizer. Q^{-1} can be determined by measuring either the width of the lorentzian response in forced vibration, or the free decay of the natural vibration.

4. Elastic constants

The elastic constants of a-Se have been determined from ultrasonic measurements by numerous authors (see review [16]). In the low frequency range (f≤1 Hz) only shear modulus G(T, f) have been reported [19,20,21].

As it is clear from Figure 5, the shear modulus G(T) commences its fall towards zero with increasing temperature before the tensile modulus. It seems from the results presented in [21] that the differences in the temperatures where the falls start are not primarily due to time scale effect. It can be assumed, as in [21], that the complex microstructure of amorphous selenium (which leads to the bimodal stress relaxation spectra) also gives rise to rather different response times to external factors.

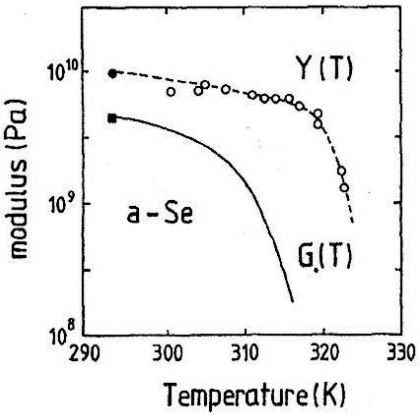

Fig. 5. Tensile modulus Y(T) and shear modulus G(T) of amorphous selenium [21].

It is established that a completely equilibrated structural state can be achieved by heating (annealing) a-Se to temperatures above T_g (≈310 K), irrespective of the previous thermal history [22-24]. Clearly, the time required to relax the initial stress increases rapidly with annealing time (fig. 6). It is necessary to note that the slow equilibration process affecting the long-time component of the stress relaxation function is also presented. The stress relaxation function can be described by Kohlraush function [25]

$$Y(T) = Y_1 \exp\left[-(t/\tau)^{\beta}\right] + Y_2 . \qquad (11)$$

Here the relaxation of the tensile stress is characterized by: **(a)** relaxation time τ; **(b)** fractional exponent $\beta \leq 1$. $Y(0) = Y_1 + Y_2$ and Y_2 are the Young's modulus for $t \to 0$ and $t \to \infty$, respectively. Equation (11) yields a straight line with slope β (the fractional exponent) in $\log_{10}\left[-\ln Y(T)/Y(0)\right]$ versus $\log_{10} t$ representation (Fig. 7).

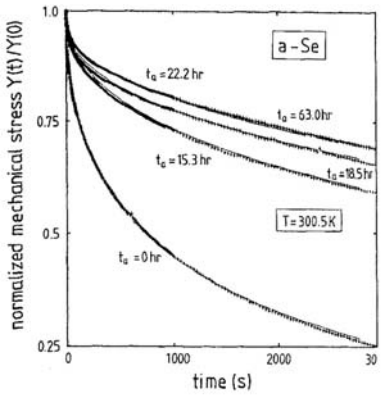

Fig. 6. Tensile stress of a-Se. The sample was previously quenched from an equilibrium state (annealing at 335 K). The time at which measurement have been started relative to the time of commencement of the first run is indicated [21].

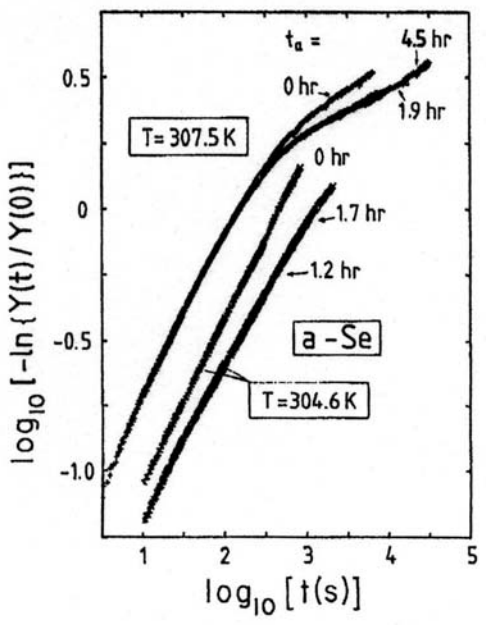

Fig. 7. Tensile autocorrelation functions of a-Se. Temperatures T and annealing time t_a (in hours after starting the first run) are indicated near the curves [21].

The slope of these curves, as seen from Figure 7, is slightly greater in virgin (unannealed) than in the annealed state.

The shear modulus measured at f=0.01 Hz behaves in a manner shown in Fig. 8 and 9, respectively. Obviously, this physical parameter is frequency-insensitive for both systems.

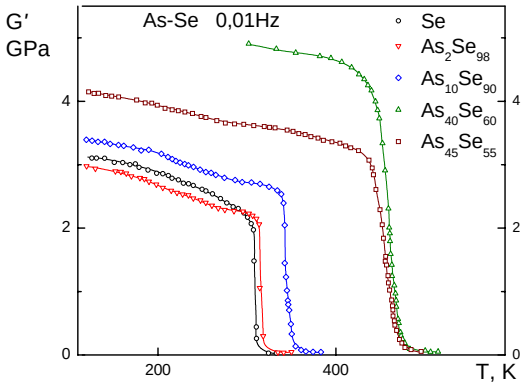

Fig. 8. Temperature dependence of shear modulus in a-As_xSe_{100-x}

The mechanical response of bulk (melt-quenched) amorphous selenium after external perturbations of two types – bending strains and temperature steps - may be summarized as follows. **(1)** The isothermal mechanical spectra indicate the presence of two relaxation processes which have distinctly different time scale and different spectral shape. **(2)** The nonlinear structural response studied by using large temperature steps as perturbations show that the two relaxation processes are governed by different equilibration dynamics. Although there are several possibilities for the assignment of the above processes, the most realistic is based on structural model now accepted [3,4].

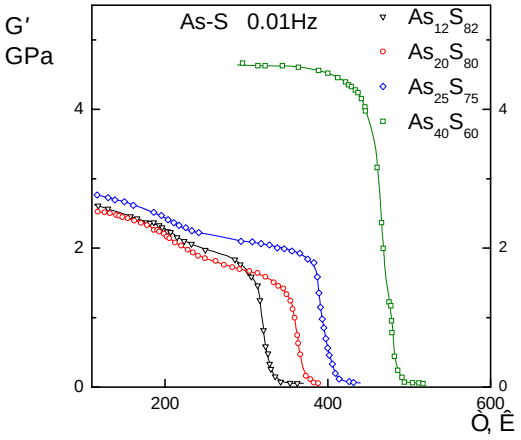

Fig. 9. Temperature dependence of shear modulus in a-As_xS_{100-x}

It seemed reasonably to assume that the two relaxation processes originate from the presence of two constituents in the molecular structure of amorphous selenium, namely chain-like segments and ring-like fragments. Therefore, in such a situation one (the first, as we suppose) of the relaxation processes can easily be suppressed or enhanced by modifying (changing) the structure of amorphous selenium. The most efficient way in this context is to change the structure of material by certain additives. Among the later, arsenic and antimony are known to be very effective branching additives which increase the degree of cross-linking of Se chain segments (see [3-5] and Refs. therein).

The existence of an internal friction peak in amorphous selenium has been reported in a series of articles by Duquesne and Bellessa [18,26-28]. Their results were obtained at 100 MHz and 10 kHz.

We present here our results on shear modulus (Figs. 8,9) and internal friction (Figs. 10,11) measured at infra-low (0.01 Hz) frequency. Preliminary data on internal friction and shear modulus in pure and alloyed Se(S) has been published earlier [29-31]. Fig. 10 and Figure 11 shows the average results obtained for As_xSe_{100-x} and As_xS_{100-x} tested systems, respectively. In general, the results obtained for the studied glasses are qualitatively similar. It clearly appears that there are two internal friction peaks in the spectra: the first one is broad and weak (Q^{-1}~10^{-3}) with location below glass transition temperature (T_{max1}~225 K; T_g≈310 K for the case of pure a-Se) – this is the so-called β process, and the second, well-defined, relatively sharp and high intensity peak. The later locates above the glass transition temperature (e.g., T_{max2}≈T_g+8 K for a-Se).

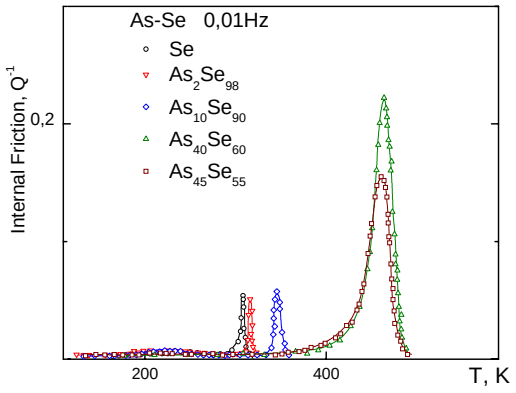

Fig. 10. Variation of internal friction with temperature in amorphous Se-based alloys.

The high temperature peak dominates in the spectrum: its intensity is ~10^2 times greater than the low temperature peak. This property, namely the presence of two peaks at least, is quite usual as far as polymers are considered. In fact, most polymers have a complicated internal friction spectrum revealing various kinds of activation processes [32].

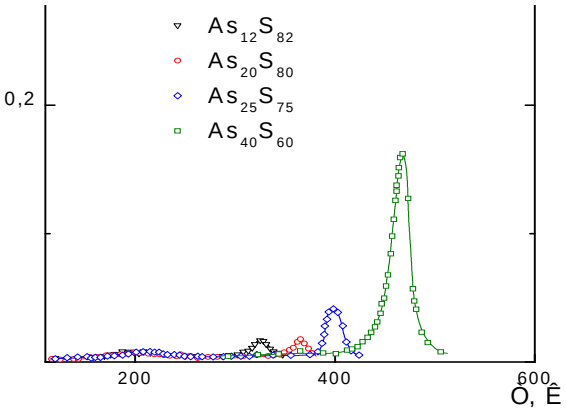

Fig. 11. Internal friction versus temperature in amorphous As_xS_{100-x} alloys.

This property, as the authors believed, could not be deduced from the high frequency data. Although the high frequency experiments reveal only one internal friction peak below the glass transition, this does not mean at all that there is only one kind of thermally activation process in As_xSe_{100-x} and As_xS_{100-x}. Duquesne and Bellessa also accentuate on such a peculiarity for the case of pure amorphous selenium [18,26-28]. Indeed, there is a strong argument in favor of this peculiarity: while a high frequency experiment in amorphous polystyrene [32] shows a single internal friction peak, the low-frequency studies have revealed three additional peaks often referred to as δ, γ, β, α (α stands for the glass transition) with increasing temperature.

Another characteristic feature of the internal friction observed in As_xSe_{100-x} and As_xS_{100-x} alloys is the location/position of the peak. Clearly, the peak in the internal friction for As_xSe_{100-x} amorphous alloys shifts to higher temperatures with arsenic content, as exemplified by Fig. 12. Therefore, the activation energy increases with As content. Another characteristic feature is that the low-temperature, β-peak, completely disappears as As content is more than 20 at%. The change in the amplitude of β-peak for compositions where it is detectable (x< 20 at% As) can not be taken into account because of the strong influence of second, α-peak. In other words, the β-peak is superimposed on the low-temperature wing of the α-peak. Generally, the peak width is important parameter which usually can be attributed to the distribution of activation energies. Despite the slight visual broadening of the β-peak, any interpretation of the above peak broadening with increasing As concentration seems to be not correct for the same reason.

The activation energy of relaxation process responsible for the first (β) peak in a-Se is $E_\beta \approx 0.35$ eV while E_α estimated for the second one is 5 times greater. The later we considered to be fictive because τ value estimated from the Arrhenius plot is unrealistic. Relaxation times determined from $Q^{-1}=f(T)$ frequency shift are $\tau_{max1}=10^{-15}$-10^{-16} s.

Figs. 12÷19 summarized results obtained for the internal peak position and height in a-As_xSe_{100-x}, a-Sb_xSe_{100-x} and a-As_xS_{100-x}.

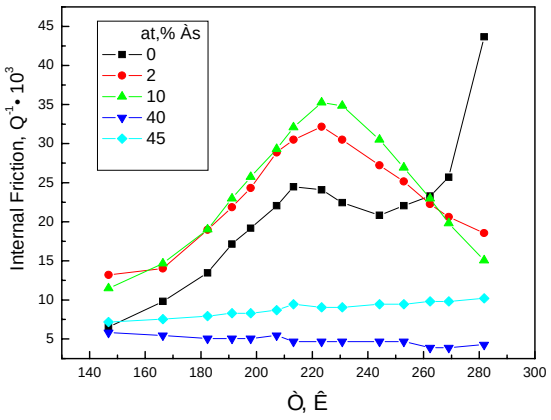

Fig. 12. β-peak in the internal friction of As_xSe_{100-x} amorphous alloys.

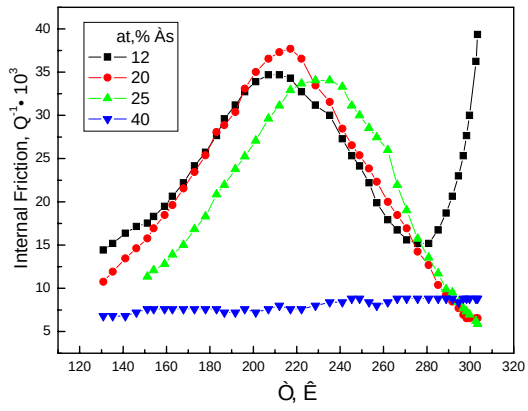

Fig. 13. β-peak in the internal friction of As_xS_{100-x} amorphous alloys.

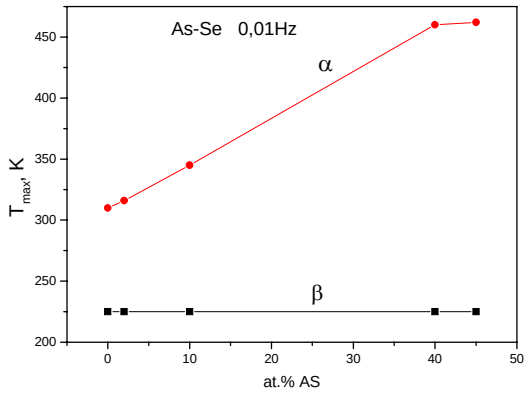

Fig. 14. The peak temperature versus As content in a-As_xSe_{100-x} for β and α processes. Lines are guides for eyes.

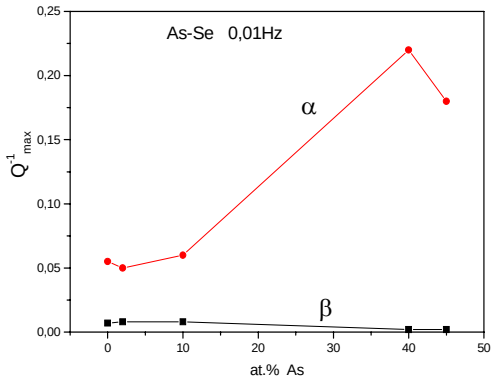

Fig. 15. The peak height versus As content in a-As_xSe_{100-x}. Lines are guides for eyes.

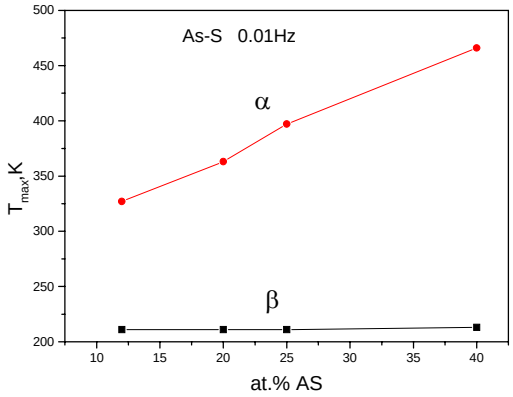

Fig. 16. The peak temperature versus As content in a-As_xS_{100-x} for β and α processes. Lines are guides for eyes.

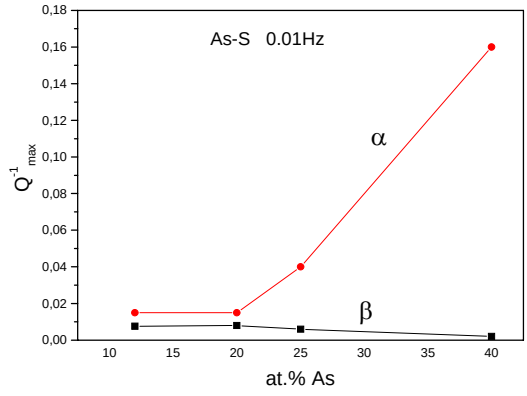

Fig. 17. The peak height versus As content in a-As_xS_{100-x}. Lines are guides for eyes.

The results obtained for Sb_xSe_{100-x} glasses revealed two well-defined peaks in the internal friction spectra: the first one (the α peak) close to the glass transition temperature, and the second (the α_c peak)– near the crystallization temperature [15]. It seems that the β-peak in the internal friction with location at $T_{max}<T_g$ was not detected by these authors. The resonance frequency plots were also shown in Fig. 18. They shift to lower temperature as the Sb content increases.

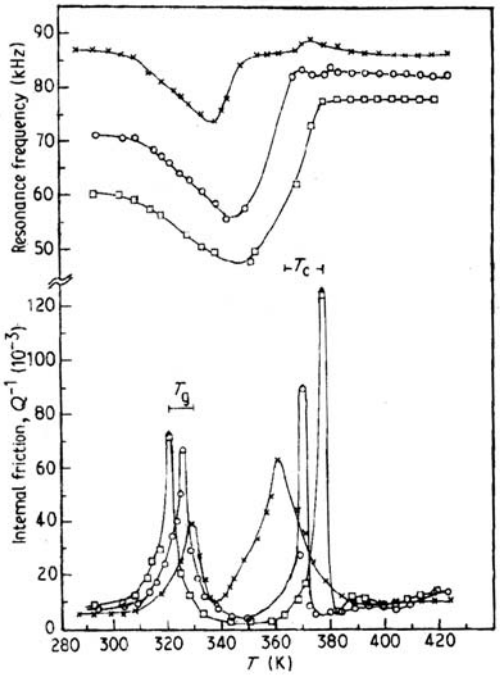

Fig. 18. The peaks observed in the internal friction (resonance frequency) in Sb_xSe_{100-x} glasses. x= 7.5 (open squares), 12.5 (open circles) and 17.5 (crosses) [15].

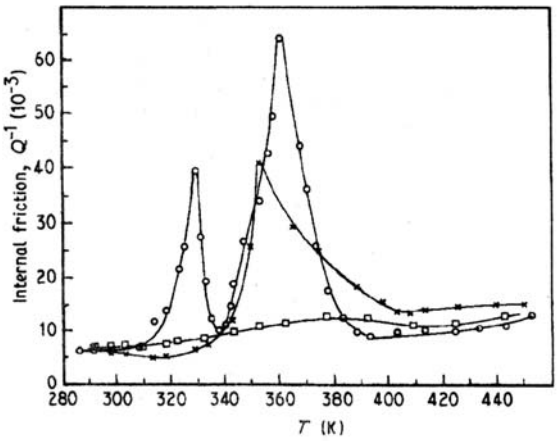

Fig. 19. Effect of annealing on the internal friction peaks observed for the $Sb_{17.5}Se_{82.5}$ system [15]. Run: (open circles)-first, (crosses)-second, (open squares)-third.

Non-crystalline selenium is one of the simplest low-weight inorganic polymers. The vitreous (glassy) modification of Se can be readily produced in the form of large samples provided that the crystallization promoting impurities can be eliminated by quench cooling the melt with sufficiently high rate. The critical rate is about 20 °C min^{-1}. The glass transition temperature of such samples is about 40 °C.

Undoubtedly, this unique non-crystalline semiconductor is an excellent starting point for further consideration of results presented. Amorphous selenium has been extensively studied over the past 70 years. Nevertheless, its molecular structure is still disputable. For a long time it was believed that the amorphous phase consisted of selenium chains, Se_n, and selenium rings, Se_8, structures mixed together. This model arose from the fact that in the crystalline phase, selenium can exist in two forms, hexagonal (trigonal) Se (γ-Se) and monoclinic Se (Se_8). Here we note that differences in the local environment around a Se atom bond length and bond angle are very small for rings and chains. Regarding mentioned structures in a-Se, the former consisted of Se_n chains and the latter of Se_8 rings. Reasonably, one can consider a structure for the amorphous phase based on a mixture of ring and chain members - both chains and eight-member Se_8 rings coexist in a-Se. However, the length of the selenium chains is uncertain. In addition, it is unclear whether a-Se contains cyclic structure or rings. As evidenced from Raman data [22, 23, 33-37], the polymer content is the dominant species of selenium's structure at any temperature. Most of these chains are found in a highly disordered arrangement but there is also a non-negligible portion of closely packed chains with strong interchain interaction.

Based on structural studies of pure and alloyed selenium, Lucovsky proposed so-called "random chain model" with existence of *cis* and *trans* linkages [38]. According to this model, all the atoms are in twofold coordinated chain structure; the dihedral angle Φ defined as the angle between two adjacent bonding planes (see Fig. 20) is constant in magnitude but changes in sign randomly.

A recent Raman scattering study performed by Yannopoulos [37] have shown that the monomer content does not exceed 15% close to the glass transition temperature of vitreous selenium.

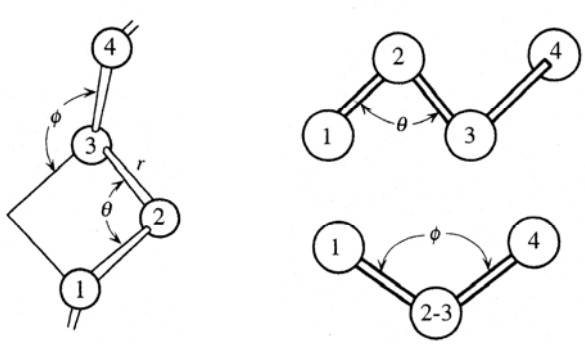

Fig. 20. Chain molecule of Se and definition of the dihedral angle [4].

The change in the sign of the dihedral angle Φ leads to ring-like or chain-like regions. Which of the above regions is realized depends on a particular sequence of the dihedral angle. If + or – is used to indicate the relative phase of the dihedral angles between the adjacent bonding planes, then a sequence of the type +–+–+ has been termed a ring-like and a sequence + + + or – – – chain-like [38]. Figure 21 illustrate the local order symbolized by + + +– + – + – – –.

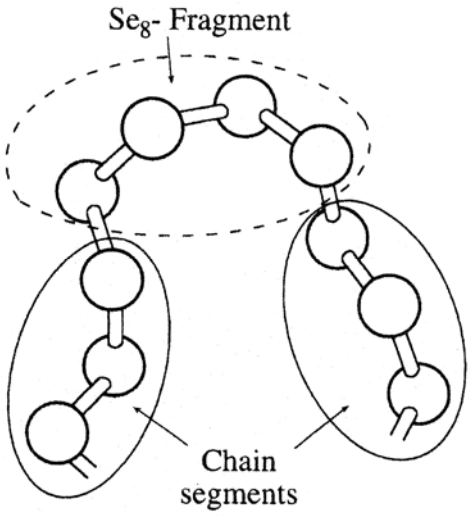

Fig. 21. Local molecular order in a selenium chain in which there are segments characterized by repetition of the same dihedral angle ("chainlike" in the sense of trigonal Se) and fragments characterized by alternating dihedral angle ("ringlike" in the sense of Se_8 molecule) [38].

One of the most recent attempts to explain the structure of non-crystalline forms of selenium and their transformations with temperature, time, etc. is due to Minaev and his concept for the polymeric-polymorphoid structure of the glass [39]. According to this concept, all forms of non-crystalline selenium are constructed of copolymerized in the greater (vitreous Se) or lesser extent (the other noncrystalline forms of Se) structural fragments of crystal lattices (polymorphoids) of trigonal, monoclinic and sometimes rhombohedric modifications without a long range order. Thus chain structures are formed. Some segments of these chains will have the *trans* configuration characteristic for trigonal selenium, while other segments will have the *cis*-configurations characteristic for Se_8 and Se_6 ring molecules from which the monoclinic and the rhombohedric modifications of selenium are built. The average coordination number for amorphous selenium is about 2.2. This means that some of the chains form "stars", in which threefold and fourfold coordinated selenium atoms are located. Besides the chain structures the non-crystalline selenium contains, in the greater or lesser extent, separate eight-member and six-member ring selenium molecules.

The concentration ratio of different polymorphoids is a fundamental characteristic of condensed selenium. Under factors like irradiation, pressure, temperature, time etc., the inter-transformation takes place between the polymorphoids of different polymorphous forms and the ratio of the concentration of different polymorphoids is altered. It seems that the non-equilibrium selenium "**memorizes**" all inherited crystalline modifications and relaxes in the direction of formation of polymorphoids of the crystal modification stable under the given conditions. Undoubtedly, trigonal selenium is the most stable modification.

Although Minaev's concept is not well established, it is capable of explaining many structural properties and experimental facts related to different transformations of the non-crystalline forms of Se including the effects of temperature and ageing (see analysis by Jannopoulos [37] for details).

The presence of β-peak in the internal friction of pure a-Se can be attributed to the existence of under-coordinated Se atoms (at the chain ends). These structural defects possibly change their space orientation into alternative one. The bond length and the valence angle θ remain constant, but the dihedral angle Φ changes during transformation. From a phenomenological point of view the microscopic processes responsible for the internal friction here considered appear as activation processes. A model involving nearly constant distribution of relatively low activation energies is able to account for the temperature location of the peak. Therefore, the β-peak in the internal friction of a-Se, as we believe, is closely related to defect structural species (chain ends). The process may be also called micro-Brownian motion of the a-Se chains leading to their best/optimum orientation.

The second internal friction peak (α-peak) detected for all a-Se specimens is attributed to the glass transition. This is connected with more extended structural species. Some of the molecular selenium chain segments are free to move, while others are not. A frozen-in segment store much more energy (for a given deformation) than can a free-to-move segment. If frozen-in species becomes free, excess energy is dissipated as heat.

The internal friction spectrum is very sensitive to the cross link density caused by As, Sb (see data presented). Several factors should be mentioned in this regards.

(1) The mean length of the polymeric units between crosslink decreases.

(2) The rigidity of the network increases.

(3) The density of crosslink increases.

The above mentioned factors have a radical influence on the internal friction properties and, at the same time, emphasize the fundamental importance of polymeric structure. Moreover, the processes here considered (which are closely related to the polymeric structure) are independent of chemical nature of elemental or binary Se(S)-based inorganic polymers.

It is known [40] that As is an effective additive to decrease the tendency to crystallize. Our experimental results, namely Raman scattering data for a-As_xSe_{1-x} films [22], indicate that the addition of As effects the suppression of the crystal nucleation and growth in a-Se. The long Se chains in a-Se branch at the site of As atoms. The length of Se chains becomes short and the a-Se cannot easily crystallize with increasing As concentration.

The As-Se system displays main extrema of various properties at the stoichiometric composition (the mechanical and chemical thresholds coincides at $x = 0.40$). There seem to exist (see Refs. cited in [5]) an additional threshold at $0.06 \leq x \leq 0.12$. It can be argued that the non-monotonic behavior observed in the concentration dependence of glass transition temperature, density, internal friction, etc. in this range originates from changes in bond topology [41]. We assume that in Se-rich glasses the network is dominated by Se atom chains (quasi-one-dimensional network) and addition of As atoms lead to branching owing to threefold coordination of As atoms. Recent publications [5, 22-24, 41], as we believe, give a new approach to the problem of local bonding in amorphous chalcogenides. The anomalous behavior near $x \approx 0.06$ is ascribed to the disappearance of Se_8-like segments. From the point of view of configuration, it is suggested that the number of *cis*-configurations in rings starts to decrease, so that the mediate-range correlation is modified. The considerable reduction in the vibration mode at ~112 cm^{-1} associated with *cis*-segments in ring component strongly supports this suggestion. Not

surprisingly that the β-peak in the internal friction which we attribute to Se chains disappear when as content exceeds 10at% (Fig. 12). Synchronously, the vibration mode observed at ~112 cm^{-1} in Raman spectra of As_xSe_{100-x} disappear if x>10at%.

Finally, we would like to say that essential variations in structure and in properties of amorphous Se- and S-based chalcogenides are possible depending on the origin, purity of starting material, sample preparation conditions and post-treatments of the sample such as storage conditions, annealing (Figs. 6,7), ageing, etc. Crystallization effects, evidenced by Raman data [42-44], have a strong effect (Figs. 18,19) on the corresponding peak in the internal friction.

References

[1] M. Popescu. Non-Crystalline Chalcogenides (Kluwer Academic Publishers, Dordrecht, 2000); M. Popescu, J. Non-Cryst. Solids **352,** 887 (2006).

[2] S. O. Kasap, J. B. Frey, G. Belev, O. Tousignant, H. Mani, L. Laperriere, A. Reznik, J. A. Rowlands, Phys. Status Solidi **B 246,** 1794 (2009).

[3] Springer Handbook on Electronic and Photonic Materials. Eds. Safa Kasap and Peter Cappa. (Springer, Heidelberg, 2006).

[4] S. O. Kasap, in "Handbook of Imaging Materials" edited by A.S.Diamond and D.S.Weiss (Marcel Dekker, Inc., New York, Second Addition, New York, 2002).

[5] Victor I. Mikla, Victor V. Mikla. Metastable States in Amorphous Chalcogenide Semiconductors (Springer, Heidelberg, Dodrecht, New York, 2009).

[6] P. Debye. Polar Molecules (Chemical Catalogue Co., New York, 1929).

[7] J. J. Benrow, D. J. C. Wood, Phys. Chem. Glass **4,** 161 (1963).

[8] J. J. Benrow, J.Sci.Instr. **30,** 412 (1953).

[9] S.L.Blum, J. Amer. Ceram. Soc. **38,** 205 (1955).

[10] R. L.Stephenson, H. E. McCoy, J. Sci. Instr. **39,** 54 (1962).

[11] G. M. Bartenev. Structure and Mechanical Properties of Inorganic Glasses. (Wolters-Noordhoff, Groningen, 1970).

[12] T. F. Miller, D. E. Day. Construction and Calibration of an Inverted Torsion Pendulum for Measuring Internal Friction of Glass. in: Technical Report N1 (1965) University of Missoury, Rolla, Mo, USA; L. Magalas, Solid State Phenomena **89** 122 (2003).

[13] J. F. W.Bell, J. M. Pelmore, J. Phys. Lett. E: Sci.Instrum. **10,** 1945 (1977).

[14] A. H. Khafagy, PhD thesis, Chelsea College, London University, 1985.

[15] A. H. Khafagy, M. Abo-Ghazala, M. M. El-Zaidia, A. A. Ammar, J.Mater.Sci. **26,** 3477 (1991).

[16] S. Etienne, G. Guenin, J. Perez, J. Phys. D **12,** 2189 (1979).

[17] A. S. Nowick, B. S. Berry. Anelastic relaxation in crystalline solids (Academic Press, New York, London, 1972).

[18] J. Y. Duquesne, G. Bellessa, J. Non-Cryst. Solids **81,** 319 (1986).

[19] A. Eisenberg, A. V. Tobolsky, J. Polym. Sci. **61,** 483 (1962).

[20] S. Etienne, J. Perez, S. Peytavin, M. Ribes, J. Solid State Chem. **92,** 27 (1991).

[21] R. Bohmer, C. A. Angell, Phys. Rev. **B 48,** 5857 (1993).

[22] V. I. Mikla, A. A. Baganich, A. P. Sokolov, A. P. Shebanin, Phys. Status Solidi **B 175,** 281 (1993).

[23] V. I. Mikla, I. P. Mikhalko, J. Non-Cryst. Solids **180**, 236 (1995).

[24] V. I. Mikla, V. V. Mikla, J. Mater. Sci: Mater. Electron. **20,** 1095 (2009).

[25] F. Kohlraush, Ann. Phys. **119,** 337 (1863).

[26] J. Y. Duquesne, G. Bellessa, J. Phys. C: Solid St. Phys. **13,** L215 (1980).

[27] J. Y. Duquesne, G. Bellessa, Phil. Mag. **B52,** 821 (1985).

[28] J. Y. Duquesne, G. Belessa, Phys. Lett. **107A,** 221 (1985).

[29] V. S. Bilanich, A.A.Horvat, I.D.Turyanitsa, Soviet Bul. Academy of Sci., Phys. Ser. **57,** 163 (1993) (in Russian).

[30] V. S. Bilanich, A. A. Horvat, I. D. Turyanitsa, V. P. Pinsenik, Ukranian J. Phys. **37,** 124 (1992) (in Russian).

[31] V. S. Bilanich, A. A. Horvat, Physics and Chemistry of Glasses **24**, 825 (1998) (in Russian).

[32] G. E. Roberts, D. F. T. White. The Physics of Glassy Polymers, ed. R.N.Haward (Appl. Sci. Publ. Ltd, London, 1973).

[33] M. Gorman, S.A. Solin, Solid State Commun. **18,** 1401 (1976).

[34] M. H. Brodsky, M. Cardona, J. Non-Cryst. Solids **31,** 81 (1978).

[35] P. J. Carroll, J. S. Lannin, Solid State Commun. **40,** 81 (1981).

[36] P. J. Carroll, J. S. Lannin, J. Non-Cryst. Solids **35**/**36,** 1277 (1980).

[37] S. N. Yannopoulos, K.S.Andrikopoulos, Journal of Chemical Physics **121**, 4747 (2004).

[38] G. Lucovsky. In: Physics of Selenium and Tellurium. (Eds. E.Gerlach, P.Grosse, Springer-Verlag, New-York, 1979).

[39] V. Minaev, S. Timoshenkov, V. Kalugin, J. Optoelectron. Adv. Mater. **7,** 1717 (2005).

[40] Z. Borisova. Glassy Semiconductors. (Plenum Press, New York, 1981).
[41] V. I. Mikla, Journal of Physics: Condensed Matter **9,** 9209 (1997).
[42] V. I. Mikla, I. P. Mikhalko, V. V. Mikla, Mat. Sci. Eng. **B83,** 74 (2001).
[43] J. Holubova, Z. Cernosek, E. Cernoskova, Optoelectron. Adv. Mater.-Rapid Comm. **1,** 663 (2007).
[44] O. Kostadinova, S. N. Jannopoulos, J. Non-Cryst. Solids **355,** 2040 (2009).

*Corresponding author: victormkl836@gmail.com